Modeling the effects of weathering on bedrock-floored channel geometry

Gregory S. Hancock,[1] Eric E. Small,[2] and Cameron Wobus[3,4]

Received 25 October 2010; revised 17 May 2011; accepted 1 June 2011; published 1 September 2011.

[1] Field and modeling studies suggest that bedrock channels equilibrate to base-level change through geometry and slope adjustment to imposed discharge, sediment supply, and substrate erodibility conditions. In this study we model the influence of bedrock weathering on channel geometry and slope as mean peak discharge (Q_m) and uplift rate (U) vary. We find that channels in which weathering is allowed to increase erodibility are wider, deeper, and less steep than nonweathering channels with the same initial conditions. While fixed erodibility channels maintain similar width/depth ratios regardless of Q_m or U, the width/depth ratio of weathering channels is sensitive to uplift rate. At low uplift rates, weathering outpaces erosion, and channels obtain similar width/depth ratios but are wider and less steep than fixed erodibility channels with equal initial conditions. At high uplift rates, erosion outpaces weathering and erodibility remains near the unweathered value, with channel shape and slope nearly identical to a fixed erodibility channel with equal initial conditions. Weathering channels differ most from fixed erodibility channels at intermediate uplift rates, with greater width/depth ratios and lower slopes than fixed erodibility channels with the same initial conditions. Our results support the hypothesis that cross-channel variations in erodibility created by weathering may be an important control on channel geometry and provide guidance for further testing of this hypothesis in natural systems.

Citation: Hancock, G. S., E. E. Small, and C. Wobus (2011), Modeling the effects of weathering on bedrock-floored channel geometry, *J. Geophys. Res.*, *116*, F03018, doi:10.1029/2010JF001908.

1. Introduction

[2] Erosion of bedrock-floored channels is a critical process governing the evolution of landscapes, because it (1) sets the boundary conditions for the evolution of adjacent hillslopes [*Burbank et al.*, 1996]; (2) transfers changes in base level produced by climatic and/or tectonic forcing through the landscape [*Berlin and Anderson*, 2007; *Bishop et al.*, 2005; *Crosby et al.*, 2007; *Wobus et al.*, 2006; *Zaprowski et al.*, 2001]; and (3) ultimately controls the rate of landscape response to perturbation [*Whipple*, 2004; *Whipple and Tucker*, 1999]. While substantial progress has been made on understanding bedrock erosion and longitudinal profile evolution, our understanding of the mechanisms by which channel cross-sectional geometry evolves remains incomplete. This limits our ability to develop models of bedrock channel evolution, because channel geometry controls: (1) the rate of energy loss as water moves through a cross section [*Tinkler and Wohl*, 1998]; (2) the distribution of velocity and shear stress [*Kean et al.*, 2009; *Miller*, 1991; *Turowski et al.*, 2008; *Wobus et al.*, 2006]; and therefore (3) the distribution of erosive power across the channel. A number of field-based studies suggest that adjustments of cross-sectional geometry may be as important as changes in gradient in maintaining erosion rates across longitudinal variations in rock resistance [*Montgomery and Gran*, 2001] and uplift rates [*Amos and Burbank*, 2007; *Duvall et al.*, 2004; *Turowski et al.*, 2009; *Whittaker et al.*, 2007a]. For example, both *Wohl and Merritt* [2001] and *Whittaker et al.* [2007a] find strong negative correlations between channel gradient and channel width/depth ratios that tend to focus erosive power, suggesting gradient and geometry adjust together in response to changes in substrate and uplift rate.

[3] In this paper, we explore the role of weathering in the evolution of rock-floored channel geometry and slope. We use a simplified model of cross-sectional evolution that represents the hydraulics of flow and permits exploration of the effects of weathering on cross-sectional geometry [*Wobus et al.*, 2006, 2008]. Using this model, we address the following question: Are channel geometry and slope significantly different in channels where weathering

[1]Department of Geology, College of William and Mary, Williamsburg, Virginia, USA.
[2]Department of Geological Sciences, University of Colorado, Boulder, Colorado, USA.
[3]Stratus Consulting, Incorporated, Boulder, Colorado, USA.
[4]Cooperative Institute for Research in Environmental Sciences, University of Colorado, Boulder, Colorado, USA.

0148-0227/11/2010JF001908

increases erodibility compared to channels where weathering is negligible?

2. Background

[4] Erosion in bedrock channels is accomplished through a combination of processes including suspended and bed load sediment impacts (i.e., abrasion), plucking of blocks, dissolution, and possibly cavitation [*Hancock et al.*, 1998; *Sklar and Dietrich*, 2004; *Whipple*, 2004; *Whipple et al.*, 2000]. The efficacy of each of these processes is dependent on very localized flow conditions, and the predominance of any individual process is controlled by a complex array of factors including river stage, rock hardness, rock structure, sediment load, bed cover, and prior rock degradation through chemical and physical weathering processes [*Hartshorn et al.*, 2002; *Turowski et al.*, 2008; *Whipple*, 2004]. As such, the predominant erosion process at any point on the bed may vary at scales smaller than the channel cross section, and point erosion rates likely vary over short spatial and temporal scales [*Hancock et al.*, 1998].

[5] In the most general terms, the cross-channel distribution of incision and the overall rate of bedrock channel erosion must depend on three factors: (1) the frequency distribution of floods, which, when combined with channel gradient and geometry, translates into a cross-channel distribution of the river's ability to erode; (2) the distribution of sediment cover, which can both protect the bed and provide tools to abrade it [*Sklar and Dietrich*, 2004; *Turowski et al.*, 2007]; and (3) the cross-channel distribution of bedrock erodibility associated with lithologic variability or produced by chemical and physical weathering of the bed and banks [*Montgomery*, 2004; *Stock et al.*, 2005]. A number of modeling studies have recently explored the coupled evolution of channel cross-sectional and longitudinal profile geometry [*Stark*, 2006; *Turowski et al.*, 2009; *Wobus et al.*, 2006, 2008]. The focus of these models is the prediction of the cross-channel distribution of shear stress, which can be used to estimate erosion rates. A nonuniform distribution of erosive power (e.g., shear stress) exists across channels because flow depth and velocity vary spatially and temporally [*Turowski et al.*, 2008]. Several of these modeling studies have shown that channel shape evolves to an equilibrium geometry that produces uniform rates of vertical channel lowering, even as bed-normal shear stress (and, hence, bed-normal erosion rate) varies across the channel perimeter [*Wobus et al.*, 2006, 2008]. However, modeling studies to date have not evaluated the potential role of variable rock erodibility on the equilibrium geometry and slope of bedrock channels.

[6] We hypothesize that variable erodibility produced by weathering in rock-floored channels is a critical process that must be considered to understand and model bedrock erosion and channel geometry. In locations where bedrock type and climate yield appreciable weathering, the bedrock exposed along channel margins becomes more and more erodible as weathering proceeds, until the weathered rock is eventually stripped by erosion during a flood [*Montgomery*, 2004; *Stock et al.*, 2005]. Rock in the channel center may be weathering at an equal pace, or even faster, but it is eroded more frequently given the greater inundation frequency. In this case, weathering may allow the lower and less frequent shear stress exerted at the margins to lower bedrock as quickly as in the channel center, when averaged over a long enough interval. Weathering rates might also be more rapid along channel margins relative to the channel thalweg for processes that are accelerated by periodic rock inundation and proximity to water, such as (1) mineral hydration during wetting and drying cycles [*Stock et al.*, 2005], (2) frost action on saturated rocks [e.g., *Matsuoka*, 1990], (3) oxidation of Fe^{2+}-bearing minerals, and (4) biologically enhanced weathering in depressions and fractures where plants may establish a foothold on otherwise bare rock surfaces [e.g., *Phillips et al.*, 2008].

3. Methods

[7] The model used here closely follows the approach and physics of *Wobus et al.* [2006, 2008]. We explicitly model the erosion rate at discrete points along the channel perimeter, allowing the channel to evolve to a self-formed geometry dictated by the flows passing through the channel cross section. We initiate the model by specifying an arbitrary initial geometry, and setting discharge (Q) and median grain size (d_{50}). Channel slope (S) adjusts as the channel responds to a prescribed rate of base-level lowering. In each time step, we calculate a rating curve for the channel cross section using the Chezy equation as by *Wobus et al.* [2006, 2008]. We calculate the Chezy coefficient, C, using

$$C = \sqrt{g}\ln\left(\frac{0.40R}{z_0}\right) \tag{1}$$

where g is gravitational acceleration, R is hydraulic radius, and z_o is a characteristic roughness height equal to $0.23d_{50}$ when assuming hydraulically rough flow [*Julien*, 1995]. From the rating curve, we find the value of predicted discharge, Q_h, that most closely matches the prescribed discharge, Q, specified for each time step. From this we obtain associated best fit values for R; mean velocity, $\overline{u}_h$; and cross-sectional area, A_h. The values of Q_h we obtain from the rating curve are always within a few percent of Q, and our rating curve method is computationally more efficient than determining channel geometry and velocity directly from Q.

[8] We follow the methodology of *Wobus et al.* [2006, 2008] to calculate the bed-normal velocity gradient. We assume the maximum velocity, $U_{\max,}$ is found at the flow surface in the middle of the channel (Figure 1), and we calculate $U_{\max}$ using $\overline{u}_h$ and the law of the wall. The mean velocity gradient at any point $l(x, z)$ along the channel perimeter is $U_{\max}/r(l)$, where $r(l)$ is the radial distance from the flow surface at the middle of the channel to the point $l(x, z)$ (Figure 1). We calculate the bed-normal velocity gradient at the characteristic roughness height, z_0:

$$\left.\frac{du}{dr(l)}\right|_{z_0} = \frac{U_{\max}}{z_0}\cdot\frac{1}{\ln(r(l)/z_0)}\cdot\sin(\phi-\alpha) \tag{2}$$

where ϕ and α are defined in Figure 1 [*Wobus et al.*, 2006].

[9] We calculate shear stress, τ, at each point along the channel perimeter using the square of the near-bed velocity gradient [e.g., *Furbish*, 1997]:

$$\tau(l) = \varphi\rho A_h\left(\left.\frac{du}{dr(l)}\right|_{z_0}\right)^2 \tag{3}$$

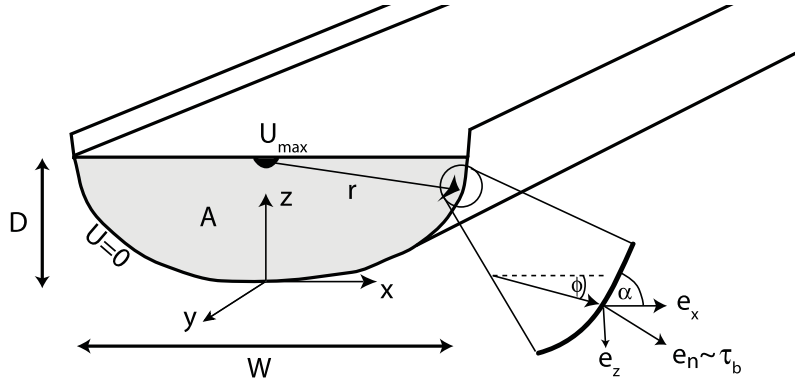

Figure 1. Schematic showing model setup, modified from *Wobus et al.* [2006]. Shear stress (τ) is a function of maximum velocity U_{max} and the distance from the channel center-top to the channel floor, $r(l)$. Bed-normal erosion rate, e_n, is assumed to be related to shear stress and is decomposed into lateral (e_x) and vertical (e_z) components using the bed inclination (α) and the angle between $r(l)$ and the horizontal (ϕ). Channel width, W, and depth, D, for a given discharge (Q) evolve during simulations.

where ρ is water density, l is the position on the channel perimeter, $du/dr(l)$ is the bed-normal velocity gradient evaluated at height z_0, and φ is a dimensionless scale factor that ensures a force balance by dictating the average shear stress along the channel perimeter is equal to the downstream weight of water [see *Wobus et al.*, 2006]. We assume the bed-normal erosion rate, $e(l)$, scales with the shear stress and rock erodibility on the bed, $K(l, 0)$, at each point:

$$e(l) = K(l,0) \cdot [\tau(l,0) - \tau_0]^n \tag{4}$$

where the exponent n could be varied so that $e(l)$ may scale nonlinearly with shear stress [e.g., *Whipple et al.*, 2000] and τ_0 is a critical shear stress threshold required before erosion can take place.

[10] A fundamental difference between the current model and previous channel geometry modeling efforts [e.g., *Stark*, 2006; *Turowski et al.*, 2009; *Wobus et al.*, 2006] is our introduction of spatially and temporally variable rock erodibility, K. In our model, we assume a uniform K for unweathered bedrock. We incorporate the effects of weathering by allowing erodibility to increase for time steps where rock is at or near the channel surface. While no accepted equation prescribes the change in erodibility as rock weathers, we attempt to capture two generally observed aspects of rock weathering: (1) weathering rates tend to decline with increasing duration of weathering [e.g., *Colman and Pierce*, 1981; *Hodson and Langan*, 1999; *Matsukura and Matsuoka*, 1991]; and (2) weathering rates tend to decline with depth below the surface [*Anderson*, 1998; *Heimsath et al.*, 1997]. Given these observations, we model the rate of change in rock erodibility, K, as a function of position l and depth below the bedrock surface, d:

$$\frac{dK(l,d)}{dt} = K(l,d) \cdot \beta(d) \cdot \left[1 - \frac{K(l,d) - K_0}{K_w - K_0}\right] \tag{5}$$

where K_0 is unweathered rock erodibility (i.e., the minimum possible erodibility) and K_w is fully weathered rock erodibility (i.e., the maximum possible erodibility). The β term captures the decline in weathering rate with depth, d:

$$\beta(d) = \beta_s e^{-d/w^*} \tag{6}$$

where β_s is the weathering rate at the surface and w^* is the weathering length scale representing the rate at which weathering falls off with depth. The term within brackets in equation (5) captures the effective duration of weathering. As weathering increases, represented by increasing rock erodibility, $K(l, d)$, the right hand term in the parentheses approaches unity, resulting in the weathering rate declining to zero as the maximum value of erodibility is approached. Using this approach, the primary influence on rock erodibility along the channel perimeter is the bed-normal erosion rate, which controls the duration of exposure to weathering. Higher erosion rates produce lower (i.e., less erodible) values of K at the bedrock surface (Figure 2).

[11] Our goal in this study is to quantify the influence of weathering on channel geometry. To this end, we describe two numerical experiments: (1) variable uplift rate with constant Q_m (variable uplift simulations) and (2) variable mean annual peak discharge, Q_m, with constant erosion rate (variable discharge simulations). In the variable uplift rate simulations, U is varied from 0.1 to 10 mm/yr with a fixed $Q_m = 20$ m^3/s (Table 1). For consistency with previous work [e.g., *Turowski et al.*, 2009; *Wobus et al.*, 2006], we use the term uplift rate to mean the rate of baselevel change, and note that equilibrium channel geometry is sensitive to relative baselevel change regardless of origin (i.e., falling baselevel or uplifting channel). In the variable discharge simulations, Q_m is varied from 2.5 to 100 m^3/s with a fixed uplift rate, $U = 1$ mm/yr (Table 1). In both experiments, we compare the equilibrium channel geometry and slope produced in simulations allowing weathering (i.e., variable erodibility) to the geometry and slope produced when there is no weathering (i.e., fixed erodibility). All simulations that allow weathering start with the same initial erodibility of K_0. The maximum value to which weathering can increase

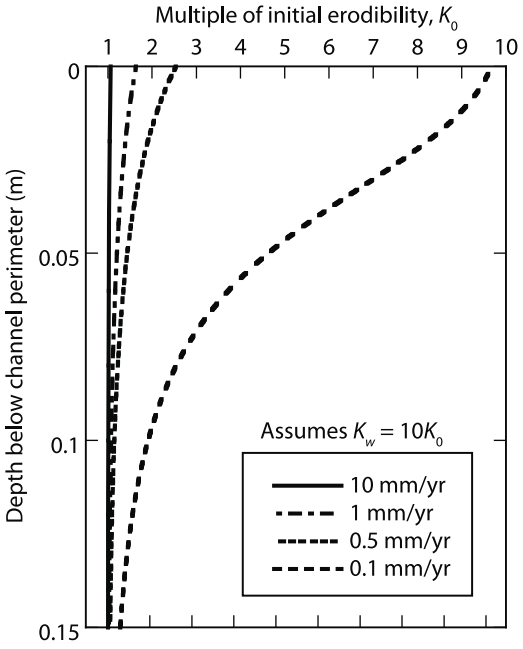

Figure 2. Equilibrium erodibility versus depth profiles predicted by equation (5) using four different erosion rates. Each calculation assumes a constant erosion rate (i.e., same rate applied at each time step) in the channel thalweg, with weathering allowed to increase erodibility up to 10 times the initial value ($K_w = 10K_0$). The x axis shows the multiple of the initial erodibility, K_0. Note high vertical erosion rates limit the amount of weathering, while low vertical erosion rates allow nearly complete weathering of rock emerging at the channel perimeter. For the case shown here, a ~100 fold decrease in erosion rate leads to a ~10 fold increase in erodibility, the maximum possible increase allowed in this example.

erodibility, K_w, is varied from 1.5 to 20 times K_0 (Table 1). In simulations without weathering, the fixed erodibility, K_f, is varied from one to 20 times K_0 (Table 1). This protocol allows us to make the following comparisons. First, we compare channels with variable erodibility, all of which have an initial erodibility equal to K_0, to the fixed erodibility channel with $K_f = K_0$. In this comparison, the fixed erodibility channel with $K_f = K_0$ represents the end-member case where weathering is completely ineffective (i.e., no change in K from initial value K_0). Second, we compare each variable erodibility channel with maximum erodibility, K_w, to the fixed erodibility channel with $K_f = K_w$. In this comparison, the fixed erodibility channel represents the end-member case where weathering increases K everywhere to the fully weathered value, K_w. Consistent with previous modeling studies [*Turowski et al.*, 2009; *Wobus et al.*, 2006], we select erodibility values that produced reasonable channel geometries and slopes over the prescribed range of uplift rates (0.1–10 mm/yr). Our choice of a maximum 20-fold increase in rock erodibility is supported by measurements showing weathering can decrease rock tensile strength, σ_T, by ~200-fold in sandstones and ~3-fold in granites [*Aydin and Basu*, 2006; *Sklar and Dietrich*, 2001]. *Sklar and Dietrich* [2001] find that rock erosion rate is proportional to σ_T^{-2}, all else being equal; hence, these measured decreases in tensile strength suggest weathering could increase rock erodibility by a factor of at least 10-fold.

[12] All other parameters in the model are kept constant for all simulations (Table 1). The maximum rate of erodibility change, β_s, and the weathering length scale, w^*, in equation (5) are 0.01/yr and 0.05 m, respectively, in all simulations. No field observations directly constrain these parameters, and we have therefore chosen values that produce channel geometries and gradients that are reasonable when compared to field observations. After presentation of these results, we discuss model sensitivity to changes in values for β_s and w^*. To obtain a consistent and physically realistic peak discharge distribution to drive channel evolution, a random number sequence was generated from a Pearson Type III distribution [*Interagency Advisory Committee on Water Data*, 1982]. The same sequence is used in all simulations presented, and the mean annual peak discharge, Q_m, is multiplied by this random number sequence to obtain the discharge time series for each simulation. Hence, channel geometries produced by a selected Q_m have been subjected to an identical discharge time series. We expect the erosion threshold, τ_0, would decrease as rock weathers, and therefore the selection of a single nonzero value for τ_0 in equation (3) is not physically realistic for simulations that include weathering. Very little data is available to appropriately constrain values for critical shear stress, and we know of no data to constrain a model to predict changes in τ_0 as rock weathers. Hence, we chose to set $\tau_0 = 0$ in equation (4) for all simulations in this initial modeling effort. For simplicity, we also set $n = 1$ in equation (3) (Table 1). All runs within each simulation set were executed for the same number of iterations (100000 with $dt = 2$ model years). In all cases presented channel geometry had reached equilibrium

Table 1. Definition and Range of Values for Key Model Parameters

Variable Name	Definition	Experiment Values: Varying Q_m	Experiment Values: Varying U	Units
Q_m	Mean peak annual discharge	2.5–100	20	m^3/s
U	Uplift rate	1	0.1–10	mm/yr
K_0	Initial erodibility in weathering simulations	0.00001		$m^{n+1}s^{2n-1}/kg^n$
K_w	Maximum erodibility in weathering simulations	1.5x to 20x K_0		$m^{n+1}s^{2n-1}/kg^n$
K_f	Fixed erodibility in nonweathering simulations	1x to 20x K_0		$m^{n+1}s^{2n-1}/kg^n$
S_0	Initial slope	0.0002		-
β_s	Maximum rate of erodibility change (equation (4))	0.01		yr^{-1}
w^*	Weathering depth constant (equation (4))	0.05		m
d_{50}	Median grain size	0.001		m
z_0	Roughness height (equation (1))	$0.23d_{50}$		m
τ_0	Threshold shear stress (equation (3))	0		Pa
n	Exponent on shear stress (equation (3))	1		-

Table 2. Results for Simulations With $Q_m = 20$ m^3/s, $U = 1$ mm/yr, and $K_w = 10K_0$ and Different Initial Cross Sections and Channel Bed Slopes[a]

Initial Cross Section[b]	Initial Slope	Width[c]	W/D Ratio[c]	Slope
V-shaped, 0.25 side slope	0.002	7.04	4.00	0.0017
V-shaped, 0.5 side slope	0.002	7.04	4.00	0.0017
20 m^3/s, $U = 0.1$ mm/yr	0.0007	7.04	4.00	0.0017
20 m^3/s, $U = 5$ mm/yr	0.009	7.07	3.98	0.0017
50 m^3/s, $U = 1$ mm/yr	0.008	7.04	4.00	0.0017

[a]Width, w/d ratio, and slope are at equilibrium.
[b]The lower three are steady state cross sections produced by the stated conditions.
[c]Values at mean peak discharge.

by the end of the simulation, operationally defined as constant average width/depth ratio observed over >1000 model iterations. In the experiments discussed, initial channel geometry is V-shaped, with channel side slope of 0.5. Following our review of model results in the discussion below, we consider further the conditions for which our model is applicable.

[13] The bed-normal erosion rate obtained from equation (4) is used to update (x, z) position for all points on the perimeter at each time step, dt. Points that define the channel margin are allowed to move in the two dimensions x, z in response to erosion. The points are frequently (here 10xdt) interpolated back onto the initial x positions to prevent growth of substantial gaps between adjacent points [*Turowski et al.*, 2009; *Wobus et al.*, 2006]. Values for erodibility are calculated simultaneously for the new x positions using a linear interpolation between points in the $K(l, d)$ matrix.

[14] Channel bed slope is determined in the model by comparing the channel thalweg elevation to a datum assumed to be located 1000 m horizontally downstream of the cross section. This datum is assigned an initial elevation value two meters below the initial channel cross section; hence, the initial slope, S_o, is 0.002 in all simulations (Table 1). At each time step in the model, we simulate relative baselevel change by lowering the elevation of this datum by the uplift rate specified for each simulation, allowing channel slope to adjust freely to the baselevel change.

[15] To ensure that initial conditions do not impact final channel geometry, we obtained equilibrium cross-section conditions from a set of simulations using different initial channel cross sections and channel bed slopes. In these simulations, we assume an uplift rate $U = 1$ mm/yr and maximum erodibility $K_w = 10K_0$. The initial channel cross sections tested include two V-shaped channels with differing side slopes of 0.25 and 0.5, and three equilibrium channel cross sections produced by the model assuming no weathering and different values of U and Q_m. The results show negligible differences between equilibrium channel sections and channel bed slopes when started with different initial conditions (Table 2), suggesting the results presented here are not sensitive to initial conditions.

4. Results

4.1. Simulations With Varying Uplift Rate

[16] Weathering produces channels with equilibrium width-to-depth ratios (W/D) that vary with uplift rate and differ from fixed erodibility channels. In both fixed and variable erodibility simulations, channel cross sections decrease in width, W, and depth, D, and channel bed slopes, S, get steeper as uplift rate, U, increases. In all simulations with fixed erodibility, the W/D is nearly constant (~3.08) regardless of prescribed values for K_f and U. In simulations with variable erodibility, W/D is sensitive to uplift rate (Figure 3). Over the experimental range of U shown in Figure 3, the W/D in variable erodibility channels is similar to fixed erodibility channels at low U, increases to a peak in W/D at intermediate values of U, and then decreases with increasing U to a W/D approaching fixed erodibility simulations. The position and height of the W/D peak is dependent on the maximum weathering allowed, with increasing K_w leading to a higher W/D peak centered at decreasing values of U (Figure 3). As we increase K_w from $2K_0$ to $20K_0$, the peak W/D increases from ~10% greater to ~50% greater than a fixed erodibility channel produced at the same U, and the position of the peak decreases from $U = 3$ to $U = 1.1$ mm/yr (Figure 3). Weathering produces a range of W/D values not observed in simulations without weathering, and the magnitude of the difference in W/D between variable and fixed erodibility channels is related to the amount of weathering allowed (K_w) and the uplift rate (U).

[17] The W/D in weathering channels is related to the difference in erodibility between the channel thalweg and the channel margins. From the range of uplift rates examined in Figure 3, we consider channel cross sections produced at low, intermediate, and high uplift rates (0.1 mm/yr, 1 mm/yr and 7.5 mm/yr, respectively) with mean discharge value $Q_m = 20$ m^3/s. We chose the intermediate uplift value to coincide with the peak in W/D when $K_w = 20K_0$ in Figure 3. Channel cross sections for six fixed erodibility simulations (K_f equal to K_0, $1.5K_0$, $2K_0$, $5K_0$, $10K_0$ and $20K_0$) and five variable erodibility simulations (K_w equal to

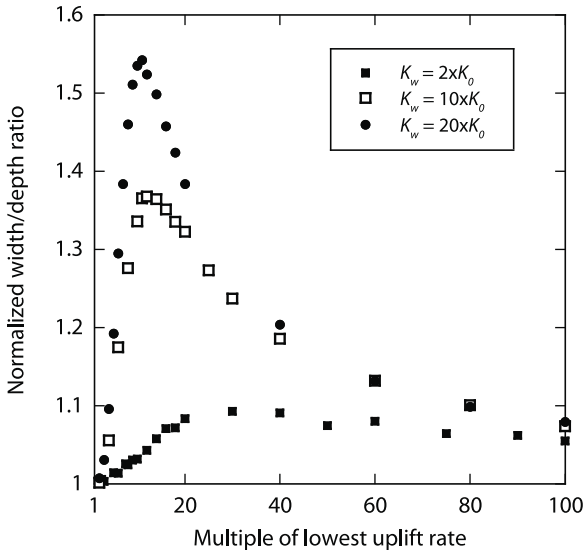

Figure 3. Normalized channel W/D at Q_m in weathering simulations with K_w equal to 2, 10, and 20 times K_0. Value on x axis is uplift rate expressed as multiple of the lowest uplift rate used in simulations ($U = 0.1$ mm/yr). We normalize W/D for these weathering simulations by dividing by the W/D (~3.08) obtained in fixed erodibility simulations.

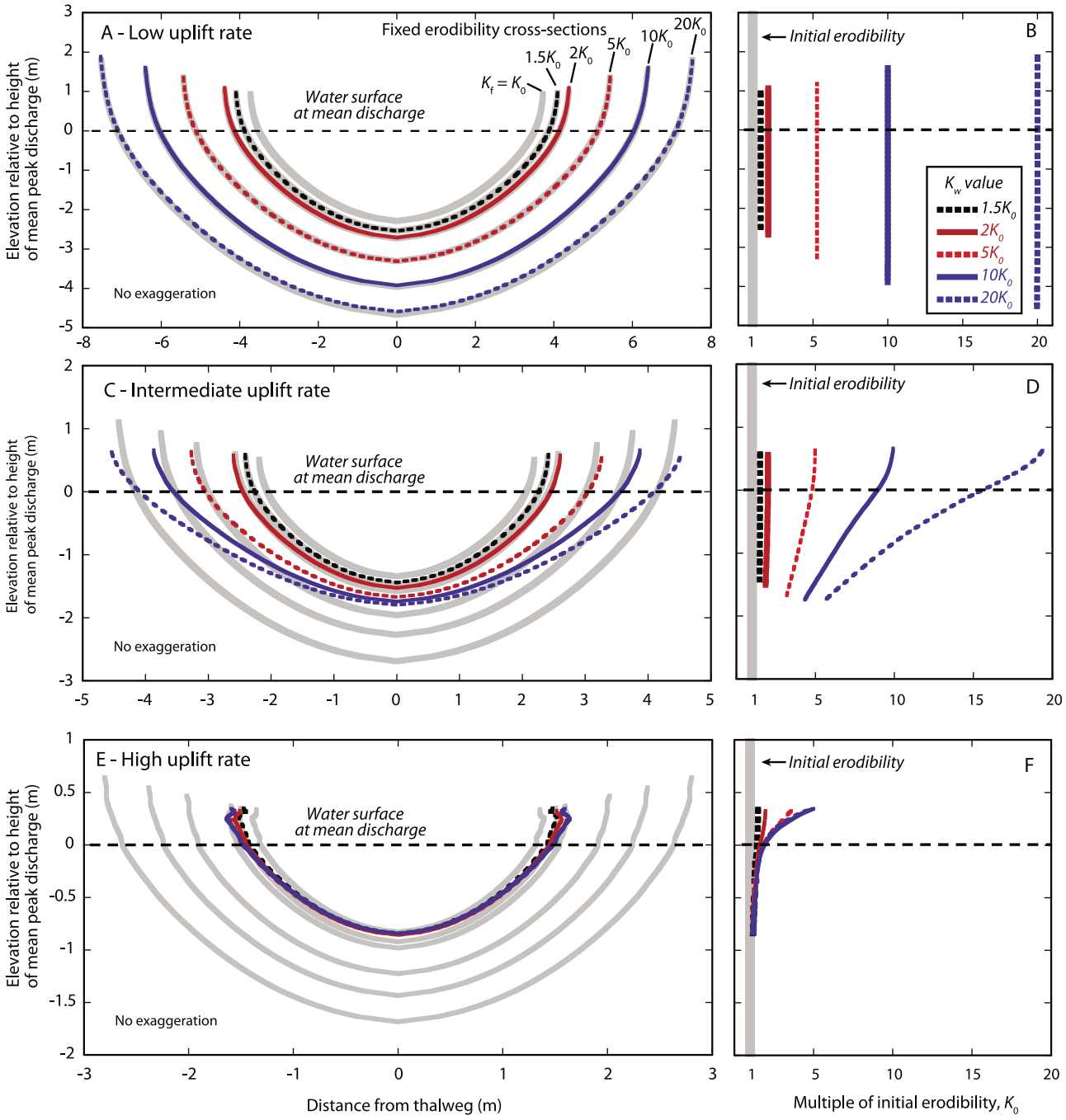

Figure 4. (a, c, and e) Equilibrium channel cross sections and (b, d, and f) rock erodibility patterns produced at low, intermediate, and high uplift rates (U = 0.1, 1, and 10 mm/yr, respectively). Mean peak discharge Q_m = 20 m^3/s in all simulations. Dashed line in cross sections denotes position of water surface at Q_m, and upper end of each cross section is the $2Q_m$ water surface height. Gray lines in A, C, and E are cross sections produced in simulations with fixed erodibility, K_f, equal to one to 20 times K_0, with increasing channel size correlated to increasing K_f. Remaining cross sections have initial erodibility equal to K_0, with weathering allowed to increase erodibility up to 1.5 to 20 times K_0 (see legend). For ease of comparison with cross sections, erodibility is expressed as a multiple of initial erodibility K_0 and is plotted as a function of elevation relative to the flow surface height of Q_m.

$1.5K_0$, $2K_0$, $5K_0$, $10K_0$ and $20K_0$) are shown in Figure 4 for the three uplift rates. At low uplift rates, the equilibrium cross sections produced in fixed erodibility simulations grow wider and deeper as erodibility, K_f, increases (i.e., gray lines in Figure 4a). In the variable erodibility simulations, all points along the channel perimeter have weathered to the maximum extent, K_w, resulting in uniform erodibility (Figure 4b). Hence, at equilibrium, the variable erodibility

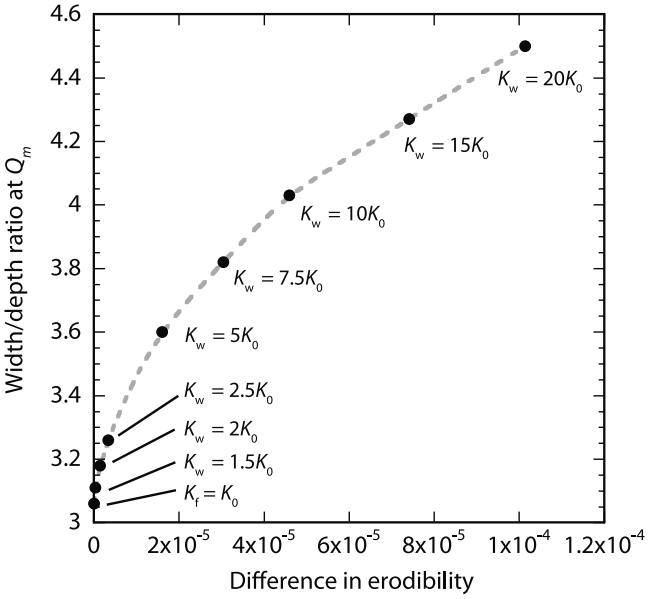

Figure 5. Relationship between W/D and difference in erodibility between the thalweg and Q_m flow height in moderate uplift rate simulations (Figures 4c and 4d). Labels show maximum allowed erodibility, K_w, as a multiple of initial erodibility, K_0, for each simulation.

cross sections (colored lines in Figure 4a) are indistinguishable from a fixed erodibility cross section (gray lines in Figure 4a) with $K_f = K_w$. At the low uplift rate, the W/D are nearly identical (~3.08) for all variable and fixed erodibility channel cross sections. When compared to the fixed erodibility channel with the same initial erodibility (gray line with $K_f = K_0$ in Figure 4a), the weathering channel cross sections are wider and deeper.

[18] At the intermediate uplift rate, cross sections produced in fixed erodibility simulations grow wider and deeper at Q_m but maintain constant W/D as fixed erodibility increases (gray lines in Figure 4c). In contrast, the variable erodibility channels increase in W/D as maximum erodibility, K_w, increases (Figures 3 and 4c). To illustrate, in the variable erodibility simulation with $K_w = 1.5K_0$ (black dashed line, Figure 4c), weathering effectiveness was sufficient to increase erodibility to the fully weathered value of $1.5K_0$ across the entire cross section (black dashed line, Figure 4d). As a result, the channel geometry is nearly identical to the fixed erodibility channel with $K_f = 1.5K_0$ (gray line directly under black dashed line, Figure 4c), similar to the result at low uplift rates. As K_w increases in the variable erodibility simulations, however, the difference in erodibility between the thalweg and channel margin increases, as shown by the increasing range of erodibility across the channel (Figure 4d). This difference in erodibility results in cross sections similar in width but shallower in depth. Therefore, W/D is higher when erodibility is variable, compared to fixed erodibility channels where $K_w = K_f$ (compare blue dashed line for $K_w = 20K_0$ to gray line for $K_f = 20K_0$, Figure 4c). As K_w increases, the difference in erodibility between thalweg and channel margin increases, resulting in greater W/D (Figure 5).

[19] At the high uplift rate, all of the weathering channels are similar in geometry to the fixed erodibility channel with $K_f = K_0$ (i.e., the simulation with the same initial erodibility as the weathering channels, Figure 4e). In the variable erodibility simulations, weathering does not increase erodibility significantly in the thalweg (K remains ~$1.2K_0$) and erodibility remains below the maximum possible value (i.e., $K < K_w$) up to a water surface height of at least $2Q_m$ (Figure 4f). The variable erodibility channels are slightly wider but similar in depth at Q_m to the fixed erodibility channel with the same initial erodibility, $K_f = K_0$ (compare innermost gray cross section to weathering cross sections, Figure 4e); hence, W/D are greater in weathering channels, as seen in Figure 3. The difference between thalweg and channel margin erodibility increases slightly as K_w increases (note increasing difference between bottom and top of erodibility curves as K_w increases, Figure 4f). As discussed for intermediate uplift rates, this increasing difference in K results in W/D increasing as K_w increases. In contrast, the size of the fixed erodibility channels increases as K_f increases (gray lines, Figure 4e) but W/D for all fixed erodibility channel cross sections again remain the same (~3.08).

[20] Equilibrium channel bed slopes increase with U for any choice of K_f and K_w. However, the response of slope to changing U in the weathering simulations differs from the fixed erodibility simulations. At all uplift rates, equilibrium bed slope decreases with increasing K_f ($S \sim K_f^{-1.2}$; Figure 6). At low uplift rates, the slope in variable erodibility channels is identical to the fixed erodibility channels with $K_f = K_w$ (low uplift rate, Figure 6). As discussed previously for W/D at low uplift rates above, the variable erodibility simulations produce cross sections with uniform values of $K = K_w$ because weathering increases erodibility to the maximum

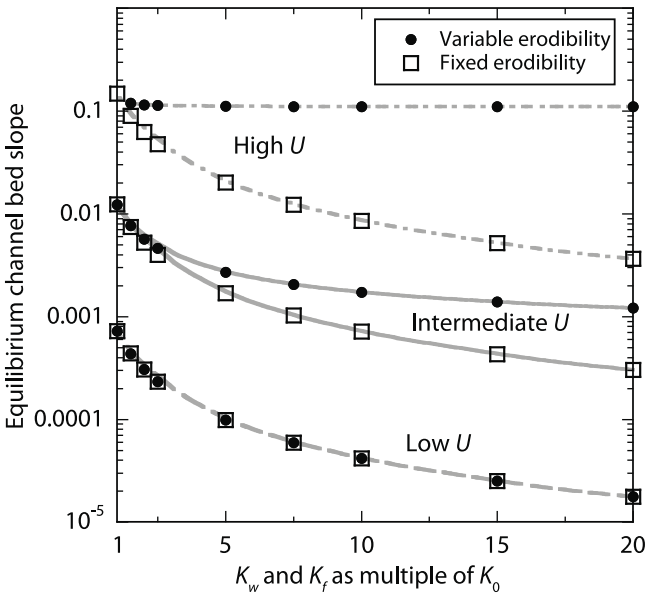

Figure 6. Equilibrium channel bed slope for variable and fixed erodibility channels in low, intermediate, and high uplift rate simulations. For ease of comparison, K_w (weathering allowed) and K_f (fixed erodibility) are expressed as multiple of K_0 on the x axis.

value everywhere in the channel (Figure 4b). Therefore, at this low uplift rate, variable erodibility channels are effectively fixed erodibility channels, with S indistinguishable from that of a fixed erodibility channel with $K_f = K_w$.

[21] At intermediate uplift rates, the slope in a variable erodibility channel decreases with K_w but remains greater than the fixed erodibility channel with $K_f = K_w$(Figure 6). The difference in slope between variable and fixed erodibility channels increases as K_w and K_f increase. As discussed previously for W/D at intermediate uplift rates, the difference in erodibility between the channel thalweg and channel margin increases with increasing K_w (Figures 4d and 5). In addition, the relative difference between the channel thalweg erodibility in a weathering channel and the fixed erodibility channel with $K_f = K_w$ increases with increasing K_w (note difference between K_w and K obtained in thalweg, Figure 4d). Therefore, at this intermediate uplift rate, as K_w increases the weathering channels are becoming relatively more resistant when compared to the fixed erodibility channel with $K_f = K_w$. This results in slope decreasing more slowly as K_w increases in the weathering channels, as seen for the intermediate uplift rate curve in Figure 6.

[22] At the high uplift rate, equilibrium slope in the variable erodibility simulations is similar for all values of K_w, while slope in fixed erodibility channels decreases (Figure 6). As discussed for W/D, at this high uplift rate, weathering does not substantially increase K above the initial value K_0 below the height of Q_m (Figure 4f). Therefore, at this high uplift rate, all variable erodibility simulations obtain an equilibrium slope similar to the fixed erodibility channel with $K_f = K_0$ (high uplift rate, Figure 6).

[23] In summary, fixed erodibility channels remain similar in geometry with increasing uplift rate, while variable erodibility channels do not. In both fixed and variable erodibility simulations, channel cross sections decrease in size and increase in channel bed slope as uplift rate increases. In fixed erodibility channels, W/D are similar (~3.08) regardless of choice for erodibility, K_f and uplift rate, U, and are hence self-similar in all simulations. In contrast, W/D of weathering channels vary with uplift rate (Figure 3). At the low end of our range of uplift rates, weathering is sufficiently effective to create uniform erodibility of $K = K_w$ everywhere in the cross section, and variable erodibility channels are nearly identical in geometry and slope to fixed erodibility channels with $K_f = K_w$ (Figures 3 and 4a). At the high end of the uplift range, weathering is only marginally effective, and all variable erodibility cross sections are nearly identical to a fixed erodibility cross section with the same initial erodibility $K_f = K_0$ (Figures 3 and 4e). At uplift rates between these end-members, variable erodibility channels reach a peak in W/D that is greater than fixed erodibility channels (Figure 3).

[24] In fixed erodibility channels, a simple power law describes the relationship between uplift rate and channel size (e.g., hydraulic radius $R \sim U^{-0.23}$; $w \sim U^{-0.23}$) and uplift rate and channel bed slope ($S \sim U^{1.23}$) for all values of erodibility, K_f. Figures 7a–7c illustrate these relationships for fixed erodibility channels with $K_f = K_0$ and $K_f = 10K_0$. These relationships are more complex in channels that weather, as the channels possess size and channel bed slope characteristics similar to fixed erodibility channels with $K_f = K_w$ at low uplift rates, and similar to the fixed erodibility control with the same initial erodibility ($K_f = K_0$) at high uplift rates. At intermediate uplift rates, the variable erodibility channels transition through channel sizes and bed slopes that are intermediate between the two end-members. For simplicity, we show uplift rate as a multiple of the minimum uplift rate, $U_{\min}$ = 0.1 mm/yr, chosen for these simulations. At uplift rates ~$3U_{\min}$, values for S, R at Q_m, and W at Q_m in the variable erodibility channel begin to deviate from the trend of the fixed erodibility channel with $K_f = 10K_0$ (Figures 7a–7c), with S increasing, R decreasing and W increasing in the variable erodibility channel. Near this uplift rate, the effectiveness of weathering varies across the channel, and the difference between erodibility in the thalweg and on the channel margin begins to increase (Figure 7d). At higher uplift rates, the difference between erodibility in the thalweg and on the channel margin increases further to a maximum difference at ~$12U_{\min}$ (Figure 6d). The maximum observed W/D for the variable erodibility channel occurs at this uplift rate (see $K_w = 10K_0$ channel, Figure 3), suggesting the difference in erodibility across the channel is an important control on W/D.

[25] The uplift rates at which the transition occurs and the magnitude of the difference in W/D between fixed and variable erodibility channels are sensitive to the choice of the weathering parameters β_s and w^* in equation (5). We expect that values for surface weathering rate, β_s, and the decrease in weathering with depth, w^*, in equation (5) would vary with field conditions (e.g., lithology, weathering processes, climate, and hydrology). Given the lack of quantitative constraints on these parameters, we explore the sensitivity of the model results to changing β_s and w^*. We completed four simulations where either β_s or w^* was varied by 10-fold above or below the value used in the simulations discussed above (Table 3). Weathering was allowed to increase erodibility by 10-fold ($K_w = 10K_0$) and $Q_m = 20$ m^3/s in all four simulations. Regardless of choice for β_s or w^*, all simulations show a peak in W/D and a transition between the end-member states comparable in magnitude to those illustrated in Figure 6. The position of the transition, however, is sensitive to β_s and w^*. As β_s or w^* is increased by 10-fold, the peak in Figure 3 and the transition in Figure 6 shift to uplift rates ~10-fold greater, and vice versa for decreasing β_s or w^* (Table 3). Hence, while the location of the transition in uplift rate space is sensitive to the choice of β_s and w^*, the transition is observed in the model results over a range of at least 2 orders of magnitude in selected values of β_s and w^*. The geometry differs most from channels with uniform erodibility when the interplay of uplift rate and weathering allows differential erodibility to develop. The specific uplift rates at which differential erodibility develops is dictated by maximum possible rate of weathering and the depth of weathering, represented by β_s and w^*, respectively, in equation (5).

4.2. Simulations With Varying Mean Discharge

[26] As mean peak discharge is varied while keeping uplift rate constant, the W/D in both fixed and variable erodibility channels remains constant. In addition, scaling relationships between Q_m and equilibrium channel characteristics (e.g., S and W) are identical in both fixed and variable erodibility channels. In this set of simulations, we vary the mean peak discharge from Q_m = 2.5 to 100 m^3/s

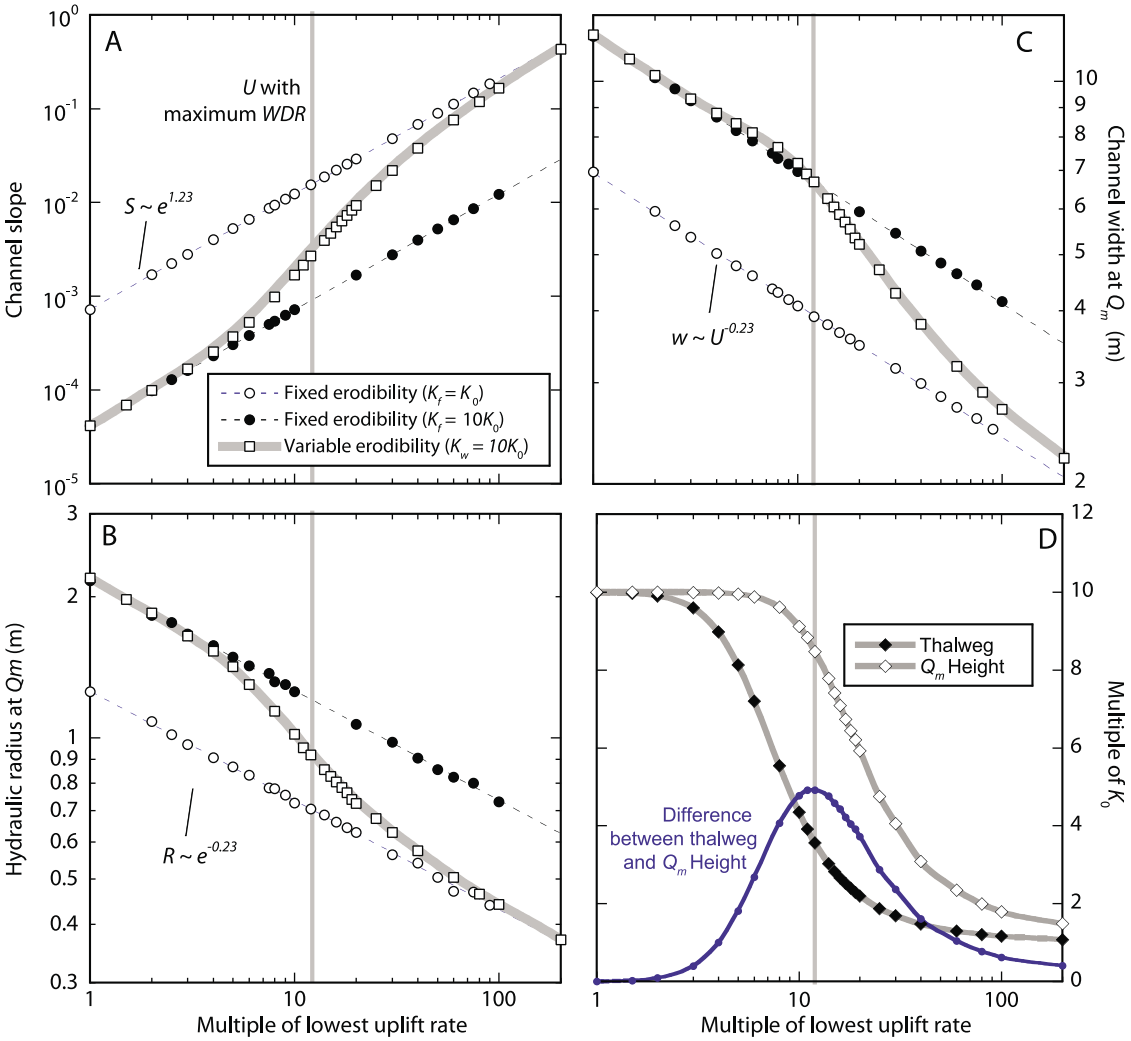

Figure 7. Equilibrium values for (a) channel slope, (b) hydraulic radius at Q_m, and (c) channel width at Q_m as a function of uplift rate. Values are shown for fixed erodibility simulations with $K_f = K_0$ and $K_f = 10K_0$ and for the weathering simulation with $K_w = 10K_0$. Value on x axis is uplift rate expressed as multiple of the lowest uplift rate used in simulations ($U = 0.1$ mm/yr). (d) Final channel margin and thalweg erodibility values and their difference expressed as a multiple of initial erodibility, K_0, for the weathering simulation with $K_w = 10K_0$. Gray line in each panel shows uplift rate producing the maximum W/D in the variable erodibility channel as shown in Figure 3.

while holding uplift rate constant (intermediate uplift rate, $U = 1$ mm/yr). We describe results at this uplift rate because the difference in W/D between fixed erodibility channels and the variable erodibility channel with $K_w = 10K_0$ occurs at this value of U, as described previously (Figures 3 and 4c). To illustrate the influence of selected Q_m, we show results from three simulations conducted at each value of Q_m (Table 1): one fixed erodibility simulation ($K_f = K_0$) and two variable erodibility simulations (K_w equal to $2K_0$ and $10K_0$). As Q_m increases in the simulations, width at Q_m increases as $W \sim Q_m^{0.5}$ and slope decreases as $S \sim Q_m^{-0.5}$ for both fixed and variable erodibility channels (Figure 8). However, W at Q_m in the variable erodibility channels is greater (Figure 8a) and S is lower (Figure 8b) than the fixed erodibility channel. For all values of Q_m, the W/D ratio remained constant for each

Table 3. Results of Sensitivity Analysis to Changing Values of β_s and w^*[a]

Value of β_s and w^*	W/D Ratio[b]	Width (m)[b]	R (m)[b]	S	U (m/yr)
$\beta_s = 0.01$, $w^* = 0.05$[c]	3.9	6.4	0.86	0.0028	0.0012
$\beta_s = 0.001$, $w^* = 0.05$	3.9	9.8	0.86	0.00028	0.00015
$\beta_s = 0.1$, $w^* = 0.05$	4.1	3.5	0.87	0.074	0.014
$\beta_s = 0.01$, $w^* = 0.005$	3.9	11	0.86	0.00028	0.00015
$\beta_s = 0.01$, $w^* = 0.5$	4.1	3.3	0.87	0.096	0.016

[a]In all simulations $Q_m = 20$ m^3/s and $K_w = 10K_0$, W/d ratio, channel width, hydraulic radius (R), slope (S), and uplift rate (U) values are taken at maximum w/d ratio in each simulation.
[b]Value at mean annual discharge.
[c]Values used for simulations shown in Figures 2–8.

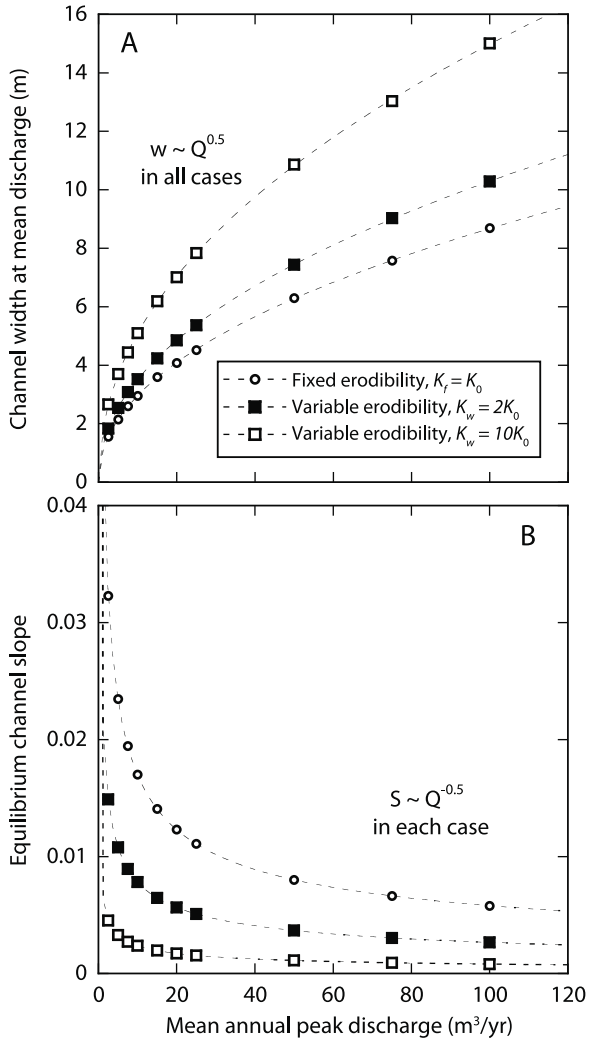

Figure 8. (a) Equilibrium channel width and (b) channel bed slope at Q_m for variable mean peak discharge experiment. Results shown for one simulation with $K_f = K_0$ and two weathering simulations with $K_w = 2K_0$ and $K_w = 10K_0$. All simulations have equal initial erodibility and have achieved equilibrium at the intermediate uplift rate, U = 1 mm/yr. As mean discharge increases, channel width increases as $Q_m^{0.5}$, with increasing weathering producing greater channel width at each value of Q_m (Figure 8a). As mean discharge increases, channel slope decreases for all simulations as $Q_m^{-0.5}$, with increasing weathering producing lower channel slopes at a each value of Q_m (Figure 8b).

erodibility simulation (3.08, 3.19, and 4.01 for $K_f = K_0$, $K_w = 2K_0$ and $K_w = 10K_0$, respectively). Hence, varying Q_m while keeping U constant produces channels that differ in absolute size and equilibrium slope, but W/D remains constant for a particular choice of K_f in fixed erodibility or K_w in variable erodibility simulations.

5. Discussion and Conclusions

5.1. The Influence of Weathering on Geometry

[27] The modeling results suggest that weathering strongly influences channel geometry and channel bed slope. The influence is complex, however, and is sensitive to the interaction between uplift rate and weathering rate. At low uplift rates, weathering outpaces erosion, allowing channel margins to weather to the maximum extent allowed in the simulation, resulting in nearly uniform erodibility along the channel perimeter (Figure 4b). The resulting channel geometry and bed slope mimic those of fixed erodibility channels with erodibility values equal to that in the weathered channel (Figures 4a, 4b, and 6). At rapid uplift rates, erosion outpaces weathering, and channel margins retain the erodibility of unweathered rock, again resulting in nearly uniform erodibility along the channel perimeter (Figure 4f). The resulting channel geometry is similar to the fixed erodibility channel with the same initial erodibility value, with the weathering channel being slightly wider and the bed slope slightly lower (Figures 4e and 6). At intermediate uplift rates, the interplay of erosion and weathering produces channels with geometry metrics (e.g., cross-sectional area, hydraulic radius, width) and channel bed slope that fall in between the two end-member uplift rates, and transition from low uplift rate to high uplift rate values as uplift rate increases (Figures 7a–7c).

[28] The W/D in weathering channels is most different from fixed erodibility channels at the uplift rate that produces the greatest difference in erodibility between the channel thalweg and margin (Figure 7d). The uplift rate at which this maximum difference occurs is sensitive to the effectiveness of weathering, including the maximum erodibility (K_w), maximum weathering rate (β_s), and the falloff of weathering rate with depth (w^*). The uplift rate with maximum W/D shifts to higher values as K_w decreases (Figure 3) and as β_s and w^* increase (Table 1), reflecting the interplay between U and the weathering variables. All simulations show a transition between the two end-member channel states when values of β_s and w^* are varied over several orders of magnitude, suggesting this behavior is not a result unique to the values chosen.

[29] Our simulations show that increasing mean annual discharge, Q_m, while keeping uplift rate constant produces channels that become larger and less steep in all simulations (Figure 8), but does not affect W/D. Because W/D in the model is sensitive to the erodibility variation along the channel perimeter, constant W/D suggests increasing Q_m does not influence the efficacy of weathering. As in previous channel geometry modeling efforts the W/D of fixed erodibility channels is insensitive to mean discharge, and only slightly influenced by uplift rate [*Turowski et al.*, 2009; *Wobus et al.*, 2006]. Hence, the inclusion of weathering results in a substantially greater range of potential equilibrium channel geometry characteristics and bed slope than is predicted by models without weathering.

[30] The inclusion of weathering in the model produces channels with scaling relationships between equilibrium width, W, and discharge, Q, similar to those obtained in the field and in previous modeling efforts. *Whipple* [2004] suggests w in bedrock-floored channels scales with $Q^{\sim 0.3–0.5}$, similar to generally stated values for alluvial channels [*Leopold and Maddock*, 1953]. This relationship is supported for bedrock channels by field observations [e.g., *Montgomery and Gran*, 2001; *Wohl and David*, 2008; *Yanites et al.*, 2010], analytical derivation [*Finnegan et al.*, 2005], and numerical modeling [e.g., *Turowski et al.*, 2009;

Wobus et al., 2006] that suggest $W \sim Q^{0.5}$. Consistent with this previous work, our model results display a similar relationship for both variable and fixed erodibility simulations ($W \sim Q^{0.5}$, Figure 8a), implying that channels with effective weathering do not produce scaling relations that distinguish them from channels without substantial weathering.

[31] Many field studies show substantial local variability from this scaling relationship. Explanations for this deviation include width changes associated with differences in uplift rate [e.g., *Duvall et al.*, 2004; *Whittaker et al.*, 2007a, 2007b; *Yanites et al.*, 2010], variation in sediment supply and grain size [e.g., *Finnegan et al.*, 2007; *Turowski et al.*, 2009; *Wohl and David*, 2008], or changes in rock resistance [e.g., *Montgomery and Gran*, 2001; *Pazzaglia et al.*, 1998]. Our modeling results suggest that weathering provides an additional explanation for variability in channel width along river profiles, even in locations where lithology or uplift rate do not change substantially. It is reasonable to expect that the susceptibility of rock to weathering, represented in our model by the parameters K_w, β_s and w^*, varies along a channel. Variation in the field would arise from those factors influencing the efficacy of weathering, including rock properties (e.g., mineralogy, spacing of discontinuities [e.g., *Wohl*, 2008]), type and abundance of vegetation cover [e.g., *Phillips et al.*, 2008], duration and depth of sediment cover, and microclimate variations associated with valley orientation and relief [e.g., *Lifton et al.*, 2009], all of which could be expected to vary along streams. Importantly, these along-channel changes in weathering effectiveness could produce variability in channel width and other channel geometry metrics even in the absence of changes in discharge, lithology, or uplift rate.

[32] Although scaling relationships quantify channel geometry metrics in proportion to Q and U, those factors that produce specific channel geometries are less well understood. Our modeling supports the hypothesis that the efficacy of weathering could be an important control on channel geometry. To illustrate this, we focus our discussion here on width/depth ratio, W/D, which provides a better indicator of channel shape than width or depth alone. Our modeling suggests W/D remains nearly constant (~3.1) in fixed erodibility channels regardless of the value of mean peak discharge (Q_m), uplift rate (U), or erodibility (K_f). The lack of sensitivity of W/D to Q_m in fixed erodibility channels is consistent with previous modeling [*Finnegan et al.*, 2005; *Turowski et al.*, 2009; *Wobus et al.*, 2006, 2008]. The model of *Turowski et al.* [2009] does show dependence of W/D on uplift rate and erodibility, with W/D ranging from ~2.0 to ~3.1, related to the inclusion of a threshold shear stress in their model (τ_0 in equation (3)); when τ_0 is decreased their model converges on W/D ratios identical to ours. Field measurements of W/D in bedrock channels vary much more widely than predicted by these fixed erodibility models (e.g., W/D = 0.2–44, n = 47 with 33 sites >3.1, *Wohl and David* [2008]). Several explanations have been suggested for the mismatch between model-predicted and field-measured W/D, including the role of sediment supply and sediment cover, discharge distribution, substrate properties and weathering [e.g., *Turowski et al.*, 2009]. Similarly, our simulations do not reveal the 2 orders of magnitude variation in W/D observed by *Wohl and David* [2008], but the inclusion of our simple weathering rule results in W/D up to ~50% greater than channels with uniform erodibility (Figure 3). We consider this to be a substantial variation in W/D given that weathering is the only mechanism that promotes increasing W/D in our model.

[33] We conclude that W/D could be strongly influenced by weathering of rocks in channels, resulting in differences in erodibility between the thalweg and channel margins. For example, in the cross sections shown in Figure 4c, W/D is positively correlated with the difference in erodibility between the channel margin and the channel thalweg (Figure 5). This modeling result is consistent with field observations showing that weathering can weaken rock along channel margins relative to the thalweg [*Montgomery*, 2004; *Stock et al.*, 2005]. Weathering thus enhances erodibility on the margins and increases the efficacy of lateral erosion, leading to widening of the channel relative to depth (i.e., increasing W/D ratio). Differential weathering may explain why *Wohl and David* [2008] find no significant relationship between W/D ratio and substrate resistance inferred from reach-scale measurements of Selby rock mass strength. Our modeling suggests differences in substrate properties between the channel margin and the thalweg may be as important as reach-scale properties in controlling channel geometry and slope.

5.2. Model Limitations and Future Work

[34] Although the present model illustrates the potential effect of weathering, several assumptions in our model limit its applicability to a narrow range of channel conditions. The assumptions underlying the technique for calculating flow and shear stress are covered by *Wobus et al.* [2006, 2008]. Inherent in this technique is the assumption of a straight and symmetrical channel, with flow velocity highest at the water surface and channel center [*Wobus et al.*, 2006]. We assume no sediment cover, which may limit bed erosion in the thalweg when sediment supply is high, leading to the dominance of lateral over vertical erosion [e.g., *Hartshorn et al.*, 2002; *Turowski et al.*, 2008]. This effect could result in periodic channel widening relative to depth, increasing the width-to-depth ratio (W/D). The maximum potential rate of weathering in our model is assumed to be equal across the entire channel cross section. However, it is reasonable to assume that weathering rate could be enhanced along channel margins relative to the channel center through processes such as wetting and drying [e.g., *Montgomery*, 2004], vegetation-enhanced weathering [e.g., *Phillips et al.*, 2008], or frost cracking [*Anderson*, 1998]. Test simulations allowing only subaerial weathering produced channels with greater W/D ratios for a given uplift rate, U, and weathering susceptibility, K_w, than the model results we present here. We also assume that weathering rate declines exponentially with depth below the channel (equation (6)), but several studies have suggested that a humped rock weathering function with the greatest weathering rate at depth is possible [e.g., *Anderson*, 1998]. The impact of sediment cover and alternate models for the distribution of weathering are targets for future modeling efforts.

[35] Our results suggest specific field measurements that can be used to evaluate the model predictions. Rock erodibility should vary in some channels and not others, depending on rock susceptibility to weathering and erosion

rate. Strategies to assess rock erodibility and the impact of weathering include use of abrasion mills [e.g., *Sklar and Dietrich*, 2001] and calculation of rock mass strength [e.g., *Wohl and Merritt*, 2001; *Wohl and David*, 2008]. In those channels where erodibility on the margins is greater than in the channel center, our model predicts that *W*/*D* should be greater than channels with more uniform erodibility. A test of this prediction should target the relationship between the variation of rock erodibility along channel perimeters and the channel geometry observed in the field. To evaluate the role of weathering in producing variable erodibility, the extent of rock weathering should be evaluated at locations where erodibility is measured. Our model suggests weathering effectiveness is controlled by values for the erosion rate, weathering rate, weathering depth, and the upper limit of weathering-induced erodibility. To test this result, we require measurements of channel geometry and erodibility along erosion rate gradients where lithology and external controls on weathering (e.g., climate) remain constant. Finally, validation of the weathering equation (equation (5)) and measurements of the parameters are required in bedrock-floored channels. Field and laboratory studies are ongoing to complete these tasks.

[36] **Acknowledgments.** This research is supported by a grant from the National Science Foundation Geomorphology and Land Use Dynamics panel (EAR 0922026). The manuscript was greatly improved by insightful comments from Alex Whittaker and two anonymous reviewers as well as the Associate Editor. We thank students Tevis Blom, Lauren Lamp, Brendan Murphy, Joseph Quinn, and Matt Sparacino for participating in stimulating discussions on weathering in bedrock-floored channels.

References

Amos, C. B., and D. W. Burbank (2007), Channel width response to differential uplift, *J. Geophys. Res.*, *112*, F02010, doi:10.1029/2006JF000672.

Anderson, R. S. (1998), Near-surface thermal profiles in alpine bedrock: Implications for the frost weathering of rock, *Arct. Alp. Res.*, *30*(4), 362–372, doi:10.2307/1552008.

Aydin, A., and A. Basu (2006), The use of Brazilian test as a quantitative measure of rock weathering, *Rock Mech. Rock Eng.*, *39*(1), 77–85, doi:10.1007/s00603-005-0069-0.

Berlin, M. M., and R. S. Anderson (2007), Modeling of knickpoint retreat on the Roan Plateau, western Colorado, *J. Geophys. Res.*, *112*, F03S06, doi:10.1029/2006JF000553.

Bishop, P., T. B. Hoey, J. D. Jansen, and I. L. Artza (2005), Knickpoint recession rate and catchment area; the case of uplifted rivers in eastern Scotland, *Earth Surf. Process. Landforms*, *30*(6), 767–778, doi:10.1002/esp.1191.

Burbank, D. W., J. Leland, E. Fielding, R. S. Anderson, N. Brozovic, M. R. Reid, and C. Duncan (1996), Bedrock incision, rock uplift and threshold hillslopes in the northwestern Himalayas, *Nature*, *379*, 505–510, doi:10.1038/379505a0.

Colman, S. M., and K. L. Pierce (1981), Weathering rinds on andesitic and basaltic stones as a Quaternary age indicator, western United States, *U. S. Geol. Survey Prof. Pap. 1210*, 56 pp.

Crosby, B. T., K. X. Whipple, N. M. Gasparini, and C. W. Wobus (2007), Formation of fluvial hanging valleys: Theory and simulation, *J. Geophys. Res.*, *112*, F03S10, doi:10.1029/2006JF000566.

Duvall, A., E. Kirby, and D. Burbank (2004), Tectonic and lithologic controls on bedrock channel profiles and processes in coastal California, *J. Geophys. Res.*, *109*, F03002, doi:10.1029/2003JF000086.

Finnegan, N. J., G. Roe, D. R. Montgomery, and B. Hallet (2005), Controls on the channel width of rivers: Implications for modeling fluvial incision of bedrock, *Geology*, *33*(3), 229–232, doi:10.1130/G21171.1.

Finnegan, N. J., L. S. Sklar, and T. K. Fuller (2007), Interplay of sediment supply, river incision, and channel morphology revealed by the transient evolution of an experimental bedrock channel, *J. Geophys. Res.*, *112*, F03S11, doi:10.1029/2006JF000569.

Furbish, D. J. (1997), *Fluid Physics in Geology*, 476 pp., Oxford Univ. Press, New York.

Hancock, G. S., R. S. Anderson, and K. X. Whipple (1998), Beyond power: Bedrock river incision process and form, in *Rivers Over Rock: Fluvial Processes in Bedrock Channels*, edited by K. J. Tinkler and E. E. Wohl, pp. 35–60, AGU, Washington, D. C.

Hartshorn, K., N. Hovius, W. B. Dade, and R. L. Slingerland (2002), Climate-driven bedrock incision in an active mountain belt, *Science*, *297*(5589), 2036–2038, doi:10.1126/science.1075078.

Heimsath, A. M., W. E. Dietrich, K. Nishiizumi, and R. C. Finkel (1997), The soil production function and landscape equilibrium, *Nature*, *388*(6640), 358–361, doi:10.1038/41056.

Hodson, M. E., and S. J. Langan (1999), The influence of soil age on calculated mineral weathering rates, *Appl. Geochem.*, *14*(3), 387–394, doi:10.1016/S0883-2927(98)00052-3.

Interagency Advisory Committee on Water Data (1982), *Guidelines for Determining Flood Flow Frequency, Hydrol. Subcomm. Bull. 17B*, 183 pp., U.S.G.S. Off. of Water Data Coord., Reston, Va.

Julien, P. Y. (1995), *Erosion and Sedimentation*, 280 pp., Cambridge Univ. Press, New York.

Kean, J. W., R. A. Kuhnle, J. D. Smith, C. V. Alonso, and E. J. Langendoen (2009), Test of a method to calculate near-bank velocity and boundary shear stress, *J. Hydraul. Eng.*, *135*(7), 588–601, doi:10.1061/(ASCE)HY.1943-7900.0000049.

Leopold, L. B., and T. Maddock Jr. (1953), The hydraulic geometry of stream channels and physiographic implications, *U.S. Geol. Surv. Prof. Pap.*, *252*, 56 pp.

Lifton, Z. M., G. D. Thackray, R. Van Kirk, and N. F. Glenn (2009), Influence of rock strength on the valley morphometry of Big Creek, central Idaho, USA, *Geomorphology*, *111*(3–4), 173–181, doi:10.1016/j.geomorph.2009.04.014.

Matsukura, Y., and N. Matsuoka (1991), Rates of tafoni weathering on uplifted shore platforms in Nojima-Zaki, Boso Peninsula, Japan, *Earth Surf. Process. Landforms*, *16*(1), 51–56, doi:10.1002/esp.3290160106.

Matsuoka, N. (1990), The rate of bedrock weathering by frost action: Field measurements and a predictive model, *Earth Surf. Process. Landforms*, *15*(1), 73–90, doi:10.1002/esp.3290150108.

Miller, J. R. (1991), The influence of bedrock geology on knickpoint development and channel-bed degradation along downcutting stream in south-central Indiana, *J. Geol.*, *99*, 591–605, doi:10.1086/629519.

Montgomery, D. R. (2004), Observations on the role of lithology in strath terrace formation and bedrock channel width, *Am. J. Sci.*, *304*(5), 454–476, doi:10.2475/ajs.304.5.454.

Montgomery, D. R., and K. B. Gran (2001), Downstream variations in the width of bedrock channels, *Water Resour. Res.*, *37*(6), 1841–1846, doi:10.1029/2000WR900393.

Pazzaglia, F. J., T. W. Gardner, and D. J. Merrits (1998), Bedrock fluvial incision and longitudinal profile development over geologic time scales determined by fluvial terraces, in *Rivers Over Rock: Fluvial Processes in Bedrock Channels*, edited by K. J. Tinkler and E. E. Wohl, pp. 207–235, AGU, Washington, D. C.

Phillips, J. D., A. V. Turkington, and D. A. Marion (2008), Weathering and vegetation effects in early stages of soil formation, *Catena*, *72*(1), 21–28, doi:10.1016/j.catena.2007.03.020.

Sklar, L. S., and W. E. Dietrich (2001), Sediment and rock strength controls on river incision into bedrock, *Geology*, *29*(12), 1087–1090, doi:10.1130/0091-7613(2001)029<1087:SARSCO>2.0.CO;2.

Sklar, L. S., and W. E. Dietrich (2004), A mechanistic model for river incision into bedrock by saltating bed load, *Water Resour. Res.*, *40*, W06301, doi:10.1029/2003WR002496.

Stark, C. P. (2006), A self-regulating model of bedrock river channel geometry, *Geophys. Res. Lett.*, *33*, L04402, doi:10.1029/2005GL023193.

Stock, J. D., D. R. Montgomery, B. D. Collins, W. E. Dietrich, and L. Sklar (2005), Field measurements of incision rates following bedrock exposure: Implications for process controls on the long profiles of valleys cut by rivers and debris flows, *Geol. Soc. Am. Bull.*, *117*(1–2), 174–194, doi:10.1130/B25560.1.

Tinkler, K. J., and E. E. Wohl (1998), A primer on bedrock channels, in *Rivers Over Rock: Fluvial Processes in Bedrock Channels*, *Geophys. Monogr. Ser.*, vol. 107, edited by K. J. Tinkler and E. E. Wohl, pp. 1–18, AGU, Washington, D. C.

Turowski, J. M., D. Lague, and N. Hovius (2007), Cover effect in bedrock abrasion: A new derivation and its implications for the modeling of bedrock channel morphology, *J. Geophys. Res.*, *112*, F04006, doi:10.1029/2006JF000697.

Turowski, J. M., N. Hovius, M. L. Hsieh, D. Lague, and M. C. Chen (2008), Distribution of erosion across bedrock channels, *Earth Surf. Process. Landforms*, *33*(3), 353–363, doi:10.1002/esp.1559.

Turowski, J. M., D. Lague, and N. Hovius (2009), Response of bedrock channel width to tectonic forcing: Insights from a numerical model,

theoretical considerations, and comparison with field data, *J. Geophys. Res.*, *114*, F03016, doi:10.1029/2008JF001133.

Whipple, K. X. (2004), Bedrock rivers and the geomorphology of active orogens, *Annu. Rev. Earth Planet. Sci.*, *32*, 151–185, doi:10.1146/annurev.earth.32.101802.120356.

Whipple, K. X., and G. E. Tucker (1999), Dynamics of the stream power river incision model: Implications for the height limits of mountain ranges, landscape response timescales, and research needs, *J. Geophys. Res.*, *104*, 17,661-17,674, doi:10.1029/1999JB900120.

Whipple, K. X., G. S. Hancock, and R. S. Anderson (2000), River incision into bedrock; mechanics and relative efficacy of plucking, abrasion, and cavitation, *Geol. Soc. Am. Bull.*, *112*, 490–503, doi:10.1130/0016-7606(2000)112<490:RIIBMA>2.0.CO;2.

Whittaker, A. C., P. A. Cowie, M. Attal, G. E. Tucker, and G. P. Roberts (2007a), Bedrock channel adjustment to tectonic forcing: Implications for predicting river incision rates, *Geology*, *35*(2), 103–106, doi:10.1130/G23106A.1.

Whittaker, A. C., P. A. Cowie, M. Attal, G. E. Tucker, and G. P. Roberts (2007b), Contrasting transient and steady-state rivers crossing active normal faults: New field observations from the central Apennines, Italy, *Basin Res.*, *19*(4), 529–556, doi:10.1111/j.1365-2117.2007.00337.x.

Wobus, C. W., G. E. Tucker, and R. S. Anderson (2006), Self-formed bedrock channels, *Geophys. Res. Lett.*, *33*, L18408, doi:10.1029/2006GL027182.

Wobus, C. W., J. W. Kean, G. E. Tucker, and R. S. Anderson (2008), Modeling the evolution of channel shape: Balancing computational efficiency with hydraulic fidelity, *J. Geophys. Res.*, *113*, F02004, doi:10.1029/2007JF000914.

Wohl, E. (2008), The effect of bedrock jointing on the formation of straths in the Cache la Poudre River drainage, Colorado Front Range, *J. Geophys. Res.*, *113*, F01007, doi:10.1029/2007JF000817.

Wohl, E., and G. C. L. David (2008), Consistency of scaling relations among bedrock and alluvial channels, *J. Geophys. Res.*, *113*, F04013, doi:10.1029/2008JF000989.

Wohl, E., and D. Merritt (2001), Bedrock channel morphology, *Geol. Soc. Am. Bull.*, *113*(9), 1205–1212, doi:10.1130/0016-7606(2001)113<1205:BCM>2.0.CO;2.

Yanites, B. J., G. E. Tucker, K. J. Mueller, Y. G. Chen, T. Wilcox, S. Y. Huang, and K. W. Shi (2010), Incision and channel morphology across active structures along the Peikang River, central Taiwan: Implications for the importance of channel width, *Geol. Soc. Am. Bull.*, *122*(7–8), 1192–1208, doi:10.1130/B30035.1.

Zaprowski, B. J., E. B. Evenson, F. J. Pazzaglia, and J. B. Epstein (2001), Knickzone propagation in the Black Hills and northern High Plains: A different perspective on the late Cenozoic exhumation of the Laramide Rocky Mountains, *Geology*, *29*(6), 547–550, doi:10.1130/0091-7613(2001)029<0547:KPITBH>2.0.CO;2.

G. S. Hancock, Department of Geology, College of William and Mary, Williamsburg, VA 23187, USA. (gshanc@wm.edu)

E. E. Small, Department of Geological Sciences, University of Colorado, 2200 Colorado Ave., Campus Box 399, Boulder, CO 80309, USA.

C. Wobus, Stratus Consulting, Inc., 1881 9th St 201, Boulder, CO 80302-5148, USA.